nature nanotechnology

ARTICLES

PUBLISHED ONLINE: 6 SEPTEMBER 2009 | DOI: 10.1038/NNANO.2009.240

All-electric quantum point contact spin-polarizer

P. Debray[1]*, S. M. S. Rahman[1], J. Wan[2], R. S. Newrock[1], M. Cahay[2], A. T. Ngo[3], S. E. Ulloa[3], S. T. Herbert[4], M. Muhammad[1] and M. Johnson[5]

The controlled creation, manipulation and detection of spin-polarized currents by purely electrical means remains a central challenge of spintronics. Efforts to meet this challenge by exploiting the coupling of the electron orbital motion to its spin, in particular Rashba spin–orbit coupling, have so far been unsuccessful. Recently, it has been shown theoretically that the confining potential of a small current-carrying wire with high intrinsic spin–orbit coupling leads to the accumulation of opposite spins at opposite edges of the wire, though not to a spin-polarized current. Here, we present experimental evidence that a quantum point contact—a short wire—made from a semiconductor with high intrinsic spin–orbit coupling can generate a completely spin-polarized current when its lateral confinement is made highly asymmetric. By avoiding the use of ferromagnetic contacts or external magnetic fields, such quantum point contacts may make feasible the development of a variety of semiconductor spintronic devices.

Spintronics is one of the most promising paradigms for the development of novel devices for use in the post-complementary metal–oxide–semiconductor (CMOS) era[1]. It aims at developing electronic devices by simultaneous manipulation of electron spin and charge and offers the possibility of devices with high speed and very low power dissipation. However, before this objective can be achieved, ways must be found for the creation, manipulation and detection of spin-polarized currents by purely electrical means. This is a challenge facing semiconductor spintronics.

Because spin–orbit coupling couples the electron orbital motion to its spin, spin–orbit coupling is a possible tool for all-electrical spin control and generation of spin-polarized current without ferromagnetic contacts and applied magnetic fields. Considerable research has been directed towards using Rashba spin–orbit coupling[2,3] to achieve these objectives[4,5]. Despite this, there has been no reported success in experimentally achieving spin injection or control by Rashba spin–orbit coupling.

In this work, we present the first experimental study of spin–orbit coupling induced by the in-plane electric field due to the lateral confining potential of a quantum wire[6] and investigate its potential for spin injection and detection. Because this spin–orbit coupling results from the lateral electric field, we call it lateral spin–orbit coupling. It is distinctly different from Rashba spin–orbit coupling, which arises from the electric field due to the asymmetry in the confining potential of a quantum well (QW) structure. Recently, it has been theoretically demonstrated that lateral spin–orbit coupling can induce accumulation of opposite spin species on the opposite edges of a quantum wire when a current flows in it[7–9]. Such spin accumulation also results in the well-known spin Hall effect (SHE)[10,11], when a charge current in a material with large spin–orbit coupling induces a pure transverse spin current. SHE has been extensively studied theoretically[11] and observed experimentally in two-dimensional systems using optical detection techniques[12,13]. The spin current predicted by SHE has so far eluded electrical detection. The origin of SHE is not related to gradients of confining potentials.

None of the theoretical works on lateral spin–orbit coupling predicts a net spin polarization that can generate a spin-polarized current. Here, we present experimental evidence of net spin polarization in side-gated quantum point contacts (QPCs)—short quantum wires—when the confining potential of the QPC is made sufficiently asymmetric. We suggest that the net spin polarization is triggered by asymmetric lateral spin–orbit coupling and can reach nearly 100% in the presence of strong electron–electron (e–e) interaction. We present proof-of-concept numerical results obtained from non-equilibrium Green's function (NEGF) analysis[14] of a model QPC device. The numerical results explain our experimental observations in a coherent manner. Finally, we point out the potential of a side-gated quantum point contact as an all-electric generator, detector and filter of spin-polarized current.

Experimental findings

The QPCs used in this work were made from nominally symmetric InAs quantum well structures. Figure 1a shows a scanning electron micrograph (SEM) of a fabricated QPC, representative of the devices used in this work. Figure 1b shows a plot of the measured conductance at 4.2 K of a QPC device as a function of sweeping voltage V_G applied to both side gates for symmetric ($V_{LG} = V_{RG}$) and asymmetric ($V_{LG} - V_{RG} \neq 0$) lateral potential confinements of the device. This plot can be taken as representative of typical device behaviour of a number of nominally identical QPCs. Figure 1c illustrates the case when the confining potential of the QPC is highly asymmetric. Measurements made on several QPC devices gave fairly similar and reproducible results, differing only in the pinch-off voltages due to differences in the lithographic channel widths. In addition to a short plateau at conductance $G \approx G_0 = 2e^2/h$, another short plateau at conductance $G \approx 0.5G_0$ was observed in the absence of any applied magnetic field only when the lateral confining potential of the QPC was made significantly asymmetric by appropriate voltage biasing of the side gates. We designate the point P (Fig. 1c) of maximum curvature at the onset of the 0.5 plateau as the $G_{0.5}$ feature. The 0.5 plateau was also observed when the asymmetry of the confining potential was reversed by reversing the constant bias voltages of the gates.

The hallmark of ballistic electron transport in a one-dimensional electron system is the quantization of its linear conductance.

[1]Department of Physics, University of Cincinnati, Cincinnati, Ohio 45221, USA, [2]Department of Electrical Engineering, University of Cincinnati, Cincinnati, Ohio 45221, USA, [3]Department of Physics and Astronomy, Ohio University, Athens, Ohio 45701, USA, [4]Department of Physics, Xavier University, Cincinnati, Ohio 45207, USA, [5]Naval Research Laboratory, Washington DC 20375, USA. *e-mail: Philippe.Debray@uc.edu

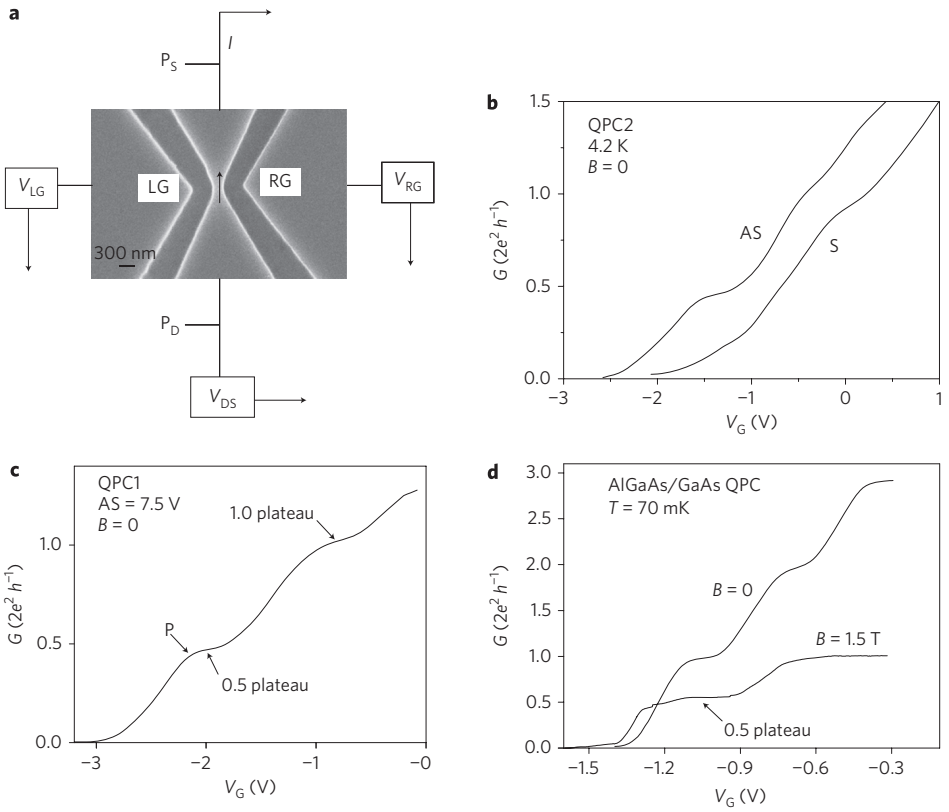

Figure 1 | Conductance *G* of quantum point contact (QPC) devices. a, Scanning electron micrograph (SEM) of the *x*–*y* plane of a typical InAs QPC used in this study. LG and RG are, respectively, the left and right side gates. The conductance of the device is determined from measurements of the current *I* and the voltage difference between the probes P_D and P_S. The arrow indicates the *x*-axis direction. **b**, Conductance of QPC2 measured in zero magnetic field *B* for symmetric (S) ($V_{LG} = V_{RG}$) and asymmetric (AS) ($V_{LG} - V_{RG} = 5$ V) transverse confining potential. The 0.5 plateau appears only when the confinement is asymmetric. **c**, Conductance of QPC1 measured at $V_{LG} - V_{RG} = \text{AS} = 7.5$ V, showing the '0.5 plateau' in the absence of applied magnetic field *B*. P is the point of maximum curvature. **d**, Conductance of a GaAs QPC, showing Zeeman spin-splitting of the first quantized conductance plateau in an external magnetic field *B*. In all cases, V_G is a sweeping voltage applied simultaneously to all gates.

The conductance is given by $G = N(2e^2/h)$, where N is the number of occupied one-dimensional subbands[15]. The factor of two on the right-hand side is the spin degeneracy of the electrons. When the spin degeneracy is removed, for example by a strong external magnetic field B, the conductance is quantized at integral values of $0.5G_0$. The Zeeman spin splitting of the first quantized plateau we have observed in the ballistic conductance of a GaAs QPC is shown in Fig. 1d. Although it is not direct evidence, the occurrence of the 0.5 plateau is considered to be a clear signature of complete spin polarization[16]. The 0.5 plateau observed in Fig. 1b,c results from spin splitting of the first quantized conductance plateau. Effects such as fluctuations and resonance due to quantum interference caused by impurities, channel wall irregularities and reflections at QPC ends do not result in a plateau in the conductance. They give rise to oscillations and/or structures superimposed on the plateaus. Moreover, such structures are suppressed in a relatively small perpendicular magnetic field[15]. The 0.5 plateau we have observed survives a fairly strong perpendicular magnetic field.

The conductance plateaus of Fig. 1b,c are not as well defined as usually observed in the quantized ballistic conductance of high-mobility QPCs (Fig. 1d). The number of plateaus observed is also quite limited. The flatness of a quantization plateau depends on the geometrical aspect ratio (W/L) of the QPC channel[17]. The smaller this ratio, the flatter the plateau. In side-gated QPCs, this ratio is fairly large, leading to less pronounced plateaus. This ratio gets larger as the QPC is opened up, driving the system to a quasi-one-dimensional state, and plateaus may no longer be visible. This explains the observation of a limited number of quantized conductance plateaus in our device. Lifetime broadening and temperature smearing at 4.2 K prevent sharp transitions between plateaus. Because we made no correction for any series resistance between the voltage probes and the QPC channel, in some devices the plateaus occur at somewhat less than the quantized values.

We believe the 0.5 plateau observed in the conductance of QPCs results from spontaneous spin polarization induced by lateral spin–orbit coupling when the lateral confinement of the QPC is made sufficiently asymmetric.

The temperature dependence of the 0.5 plateau was studied to obtain an idea of the magnitude of the spin splitting responsible for its occurrence. Lowering the temperature from 4.2 K down to 25 mK had no effect. With increasing temperature, the 0.5 plateau survived up to ~13 K (Fig. 2a). Dependence of the 0.5 plateau on drain–source bias voltage V_{DS} is shown in Fig. 2b. Conductance of the $G_{0.5}$ feature decreases as V_{DS} increases and finally the feature disappears owing to electron heating when V_{DS} increases to ~1 mV. This is fairly consistent with the observed temperature dependence that results from temperature smearing of the Fermi level.

Measurements of conductance were also made in magnetic fields applied in-plane parallel to the current and perpendicular to the device plane. Reversing the direction of the field gave identical results. Figure 3 shows typical results of the influence of magnetic field on the conductance of the QPCs. A parallel field up to 7 T had hardly any influence on the 0.5 plateau (Fig. 3a), a sign of initial ferromagnetic or fully spin-polarized state. In a perpendicular

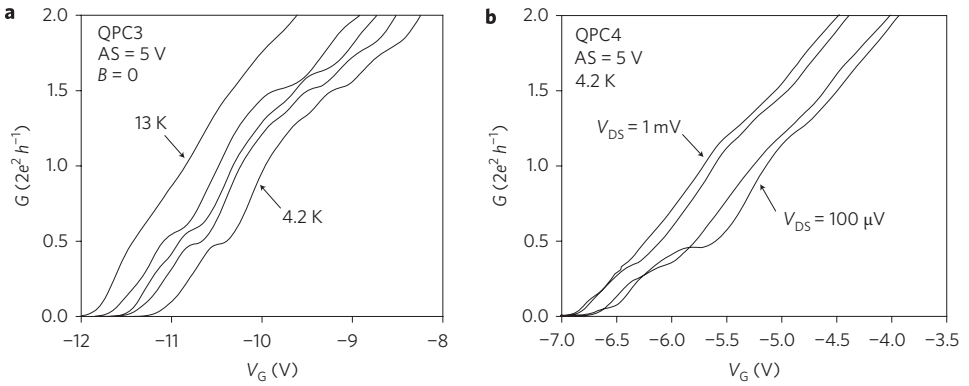

Figure 2 | Effect of temperature and drain–source bias voltage on the 0.5 plateau. a, Temperature dependence of the 0.5 plateau showing the survival of the plateau up to ~13 K. Measurements were made at temperatures (from right to left) 4.2, 6, 8, 10 and 13 K. The curves are shifted laterally for clarity. **b**, Dependence of the 0.5 plateau on drain–source bias voltage V_{DS}. From right to left $V_{DS} = 100$, 300, 600 μV and 1 mV. The plateau disappears at $V_{DS} = 1$ mV.

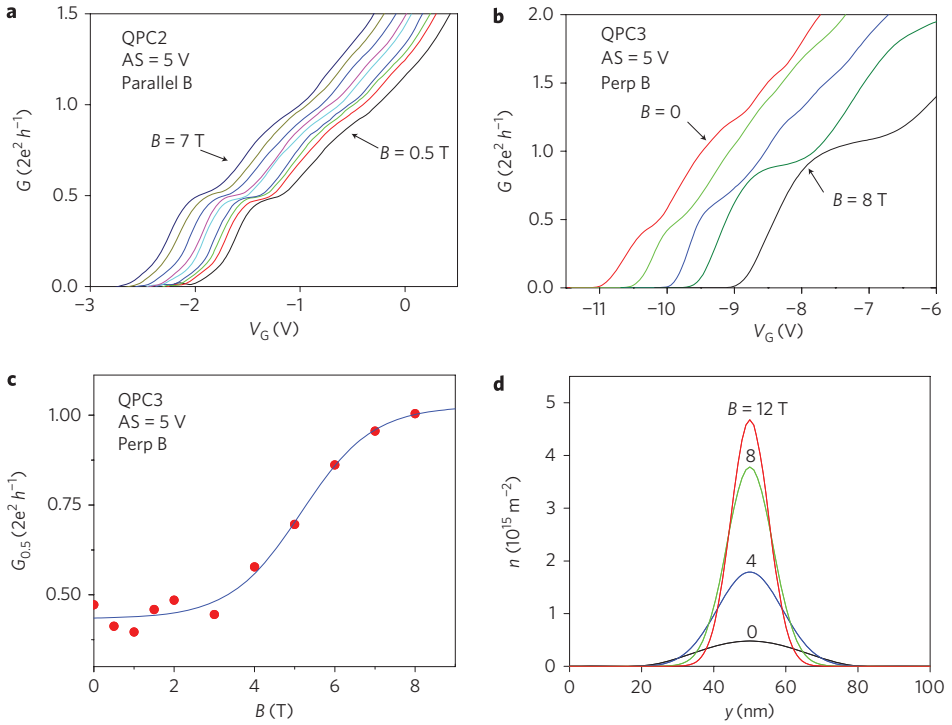

Figure 3 | Effect of applied magnetic field on the 0.5 plateau. a, Conductance of QPC2 in in-plane field B parallel to current measured at an asymmetry $V_{LG} - V_{RG} = \mathrm{AS} = 5$ V for (from right to left) 0.5, 1.0, 1.5, 2.0, 3.0, 4.0, 5.0, 6.0 and 7.0 T. **b**, Conductance of QPC3 in field B perpendicular to device plane measured at an asymmetry as in **a** for (from left to right) 0, 2, 4, 6 and 8 T. The traces in **a** and **b** are offset laterally for clarity. In both cases, V_G is a sweeping voltage applied simultaneously to both side gates. **c**, Conductance of the $G_{0.5}$ feature of QPC3 as a function of applied perpendicular magnetic field. The solid curve is a guide to the eye. **d**, Influence of perpendicular magnetic field on areal electron density in the lowest one-dimensional subband calculated for a model QPC device (see text for details) at the centre of the QPC channel. Each curve shows the variation of electron density along the transverse y-direction for a given field. The number on each curve gives its field value.

field, the plateau at $G \approx 0.5G_0$ rises with increasing field and evolves to a plateau at $G \approx G_0$ (Fig. 3b,c). The conductance of the $G_{0.5}$ feature rises simultaneously. Such dependence has not been reported before. A perpendicular magnetic field influences the orbital motion of the electrons and introduces an additional confinement, which influences the electron density in the channel (see Supplementary Information, B). In general, the electron density in a channel increases with increasing field, reaches a maximum, then decreases as the Fermi level drops below the band bottom, causing magnetic depopulation[18]. Here, we are interested in the influence of magnetic field on the electron density in the lowest one-dimensional subband when the 0.5 plateau occurs. To study this, we consider the $G_{0.5}$ feature (point P in Fig. 1c). This feature results when the Fermi level crosses the lowest band bottom from below and is just above it, irrespective of the energy of the band bottom and therefore of the magnitude of the applied perpendicular magnetic field. A model QPC with realistic confining potential $U(x,y)$ of size close to the experimental device was considered (see Supplementary Fig. S3). The Fermi level was chosen at 1 meV above the band bottom. Figure 3d shows transverse cross-sections of the areal electron density for four values of the applied perpendicular magnetic field obtained by numerical solutions. A sharp rise in the electron density is observed with increasing magnetic field. It is well known that the Coulomb e–e interaction

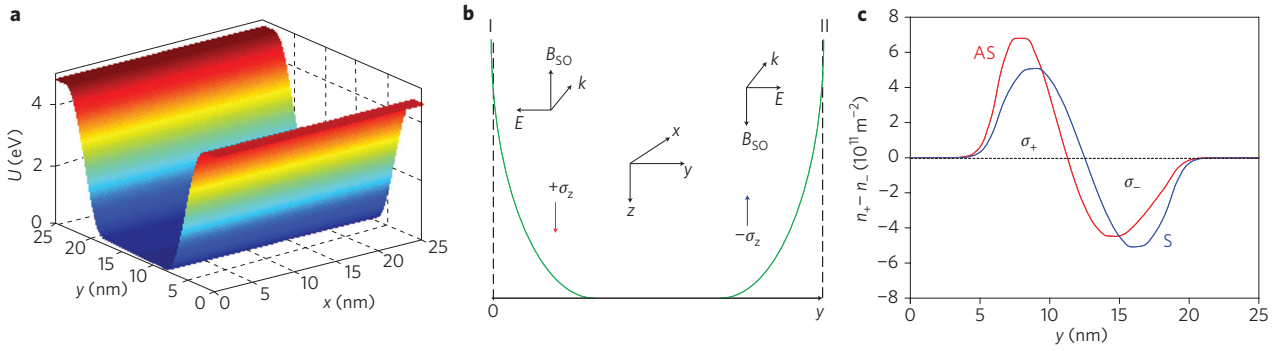

Figure 4 | NEGF computation of spontaneous spin polarization in model QPC. a, Potential energy $U(x,y)$ of a model square QPC of length L (x-axis) and width W (y-axis) equal to 25 nm used in NEGF calculations. The potential rises in a sinusoidal fashion at the transverse edges (y-axis). **b**, Schematic representation of the transverse confining potential of a side-gated QPC. The dashed vertical lines I and II represent, respectively, the left and right edge of the QPC channel. The green curve indicates the confining potential. Opposite spin species ($+\sigma_Z$ and $-\sigma_Z$) are induced by lateral spin-orbit coupling at the opposite transverse edges of the QPC channel. B_{SO} is the effective magnetic field induced by lateral spin-orbit coupling, E the electric field due to the potential gradient and k the electron propagation wave vector in the x-direction. **c**, Plot of net areal spin density at $x = L/2$ along the transverse y-direction for symmetric (S, $V_I - V_{II} = 0$) and asymmetric (AS, $V_I - V_{II} = 0.3$ V) confinement based on potential profile of **a**. Transport is in the lowest subband. A drain–source bias of 100 μV was used in the calculations. A net spin polarization is observed in the asymmetric case.

decreases with increasing electron density[19]. The rise of the $G_{0.5}$ feature with increasing perpendicular magnetic field may conceivably be related to the decrease in the e–e interaction as the electron density increases. We shall see in the following that e–e interaction in a one-dimensional system[20–22] plays a major role in the origin and occurrence of the 0.5 plateau.

Origin of the 0.5 plateau

A realistic model of the lateral confining potential $U(y)$ of a side-gated QPC device is one with a flat bottom with sharply rising walls at the edges (see Supplementary Information, C). The electrons are considered to propagate in the x-direction, along which the potential is assumed to be constant. The free-electron Hamiltonian H of the QPC is given by

$$H = H_0 + H_{SO}$$
$$H_0 = \frac{\hbar^2(k_x^2 + k_y^2)}{2m^*} + U(y) \quad (1)$$
$$H_{SO} = \beta\vec{\sigma} \cdot (\vec{k}_x \times \vec{\nabla}\, U(y))$$

In equation (1), H_{SO} is the lateral spin–orbit coupling interaction term[11], β the intrinsic spin–orbit coupling parameter of the channel material, $\vec{\sigma}$ the vector of Pauli spin matrices and m^* the electron effective mass. The effective magnetic field induced by lateral spin–orbit coupling is $\vec{B}_{SO} = \beta(\vec{k}_x \times \vec{\nabla}U(y))$, where k_x is the propagation vector along the x-direction and $\vec{\nabla}U(y)$ the spatial gradient of the confining potential along the y-direction. We have not considered any Rashba spin–orbit coupling term in H. Shubnikov de Haas oscillations measured at 4.2 K do not show any beating patterns (see Supplementary Fig. S4), indicating Rashba spin–orbit coupling is not observable in our experiments. We have also neglected the Dresselhaus spin–orbit interaction. Our measurements were made with current along the [100] direction, for which this interaction is minimum for InAs[23]. Lateral spin–orbit coupling is the only spin–orbit interaction considered. Because the 0.5 plateau occurs in the fundamental mode of transport, in all our numerical calculations hereafter we have chosen a Fermi level in the lowest one-dimensional sub-band.

A numerical solution, using a scattering matrix approach, of the free-electron Hamiltonian H did not give a 0.5 plateau in the conductance (see Supplementary Information, E). This is not surprising. The free-electron Hamiltonian H is invariant under time reversal and must have at least twofold Kramers degeneracy. The time reversal invariance (TRI) must be broken for spin polarization to be possible. The current flowing in the system due to an external bias voltage can break the TRI and lead to spin polarization.

The NEGF formalism was used to numerically solve equation (1) and calculate the spin densities along the transverse y-direction for a square model device of side 25 nm. This size was chosen to keep numerical solutions tractable. Our goal was to obtain proof-of-concept results rather than an exact solution for the experimental device. Figure 4a shows the model potential $U(x,y)$ used for the purpose (see Supplementary Information, C). Moving electrons with opposite spins experience opposite lateral spin–orbit coupling forces that displace them in opposite directions along the y-axis. This results in an accumulation of opposite spins at the opposite transverse edges (Fig. 4b). For symmetric confinement, spin polarizations at the opposite edges cancel each other, giving zero net polarization. In the asymmetric case, $+\sigma_Z$ on the left edge I predominates over $-\sigma_Z$ on the right edge II. This results in a net $+\sigma_Z$ polarization (Fig. 4c). When the asymmetry between V_I and V_{II} is reversed, the direction of spin polarization is reversed. The polarization shown in Fig. 4c is too small to cause the highly polarized 0.5 plateau. A strong e–e interaction is needed for it.

The e–e interaction was taken into account by considering a repulsive Coulomb contact potential, $V_{int}(\vec{r},\vec{r}') = \gamma\delta(\vec{r} - \vec{r}')$, where γ indicates the e–e interaction strength. A total interaction self-energy, $\sum_{int}^{\sigma}(\vec{r})$, was added to the Hamiltonian (see Supplementary Information, F). NEGF numerical calculation of the conductance of the model QPC (Fig. 4a) was carried out using the approach of ref. 19. The parameters γ and β were set, respectively, to $5.4(\hbar^2/2m^*)$ and 2.0×10^{-18} m^2. The value of γ chosen is moderate for a one-dimensional electron system and can be much higher for low electron density[19]. The value of β chosen is appropriate for InAs[11]. As we shall see later, the exact value of β is not of crucial importance. The conductance was calculated using the Landauer formula[24] for ballistic transport. Figure 5a shows, as a function of V_T, the total conductance for symmetric and asymmetric confinements. The parameter V_T is a common-mode voltage that represents an overall shift of the potential energy profile. A well-defined 0.5 plateau is observed in the asymmetric case, indicating almost 100% spin polarization. Reversing this asymmetry reverses the direction of spin polarization. The spin splitting was found to be 43.5 meV, indicating survival of the 0.5 plateau

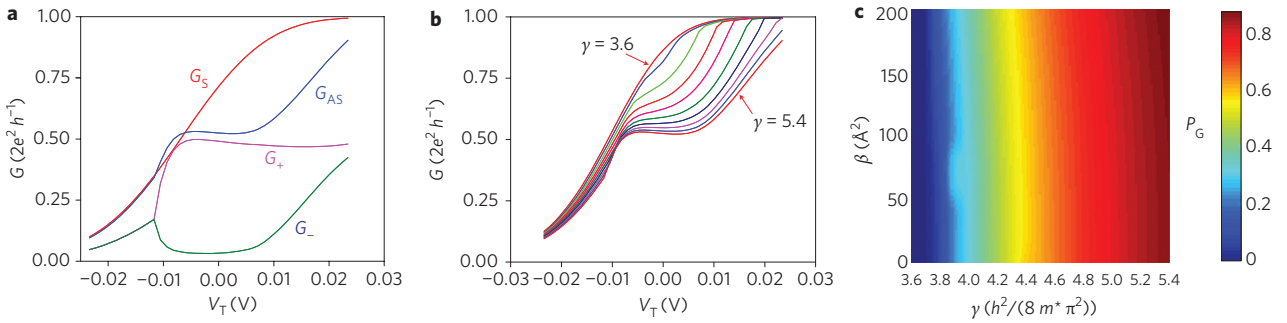

Figure 5 | NEGF computation of conductance *G* of model QPC. a, Total conductance of the model QPC (Fig. 4a) obtained from NEGF calculations for symmetric (G_S, $V_I - V_{II} = 0$) and asymmetric (G_{AS}, $V_I - V_{II} = 0.3$ V) cases. G_+ and G_- are, respectively, the conductance of electrons with spin σ_+ and σ_- for the symmetric case. V_T is a gate shift potential (see text). A drain–source bias of 100 μV was used in the calculations. **b**, Rise of the 0.5 plateau conductance with decreasing e-e interaction strength γ (from bottom to top) 5.4, 5.2, 5.0, 4.8, 4.6, 4.4, 4.2, 4.0, 3.8 and 3.6 for $\beta = 2.0 \times 10^{-18}$ m^2. **c**, Dependence of the conductance polarization $P_G = (G_+ - G_-)/(G_+ + G_-)$ on lateral spin-orbit coupling parameter β and interaction strength γ at $V_T = 0$ for $V_I - V_{II} = 0.3$ V and a drain–source bias of 100 μV.

to high temperatures. It is expected to be smaller for the larger experimental device. A quantitative comparison between the experimental results and those for the model device is difficult because the exact dimensions of the experimental device are not known. Also, because the gates of the experimental device are separated from the channel by wide trenches (Fig. 1a), to produce the same asymmetry in the confining potential a much larger voltage is needed in the experimental device than for the model device (Fig. 4a). This also explains the quantitative disparity between V_G (Fig. 1c) and V_T (Fig. 5a).

Figure 5b shows that the plateau at $G \approx 0.5G_0$ rises and evolves into a plateau at G_0 as γ decreases for a given β. This indicates the need for a large γ and therefore of a strong e–e interaction for the occurrence of the 0.5 plateau. The interaction parameter γ is inversely proportional to m^*, which is material dependent, and increases sharply with decreasing electron density, which can be engineered.

Because γ decreases with increasing electron density, this behaviour predicts a rise of the plateau with increasing perpendicular magnetic field. This is in qualitative agreement with our experimental observations (Fig. 3b,c). The spin polarization induced by lateral spin–orbit coupling is perpendicular to the device plane and its direction depends on the direction of the current (Fig. 4b). For a given current, the evolution of the 0.5 plateau with increasing field is expected to depend on the direction of the field, provided the field induces its own Zeeman spin polarization. We have not observed any Zeeman spin splitting in fields up to 8 T (see Supplementary Fig. S4). In the absence of any observable Zeeman spin polarization, reversing the field direction should have no effect on the 0.5 plateau (see Supplementary Information, B), consistent with our experimental observations.

Three ingredients are essential for the occurrence of the 0.5 plateau in a QPC: an asymmetric lateral confinement, lateral spin–orbit coupling and a strong repulsive Coulomb e–e interaction. To better understand the mutual role of lateral spin–orbit coupling and e–e interaction in the origin of the 0.5 plateau, NEGF calculations of the conductance were carried out for the model device of Fig. 4a over a range of β and γ values at $V_T = 0$. Figure 5c shows conductance polarization as a function of β and γ. It predicts the possibility of generating a wide range of spin polarization with a QPC device. It is important to point out that in all cases with $\beta = 0$, it was necessary to include a small external magnetic field to trigger the convergence of the self-consistent iteration process[19,25]. This emphasizes the need for an initial spin imbalance, however small. In our experiments, this is provided by the asymmetric lateral spin–orbit coupling.

The observation of an anomalous plateau at $G \approx 0.5G_0$ in GaAs QPCs has been reported in recent years[26,27]. The devices used were not conventional QPCs defined by two gates, but had multiple gates[26] or a complicated depletion pattern[27], making it difficult to have a clear idea of the symmetry of the confining potential when the plateau was observed. It is worth mentioning here the extensively studied 0.7 structure[28] observed in the ballistic conductance of GaAs QPCs. The phenomenon has been the subject of extensive research and great interest[29]. The experimentally observed characteristics of the 0.7 structure are distinctly different from those of the 0.5 plateau studied here (see Supplementary Information, G). A number of scenarios have been proposed to explain the origin of the 0.7 structure, such as static and dynamic (Kondo effect) spin polarization, Wigner crystallization, ferromagnetic spin coupling and so on. Its origin is still debated even after a decade of research[29]. It would be interesting to explore any possible role of asymmetric lateral spin–orbit coupling and e–e interaction in the appearance of the 0.7 structure.

Conclusion and outlook

This work shows that a side-gated QPC with low electron density, made of a semiconductor with large intrinsic spin–orbit coupling, can be used to generate highly spin-polarized current of either spin species by controlling the symmetry of its confining potential by gate bias voltages. The device can be electrically tuned on demand to transmit or reflect an incident polarized current with spin up or spin down. The QPC thus can be used as an all-electric spin polarizer, detector or filter.

It would be interesting to have direct evidence of lateral spin–orbit coupling induced spin polarization in a QPC. This can be obtained from electrical measurements of the Hanle effect in a device consisting of two QPC devices (see Supplementary Information, H).

Methods

The semiconductor structures used in this work were nominally symmetric InAs QWs, sandwiched between $In_{0.53}Ga_{0.47}As$ barriers, with a two-dimensional electron gas (2DEG) in the well. The low-bandgap semiconductor InAs was chosen as the QW material because of its large intrinsic spin–orbit coupling, more than an order of magnitude larger than that of GaAs[11]. The InAs QW structures were characterized by integral quantum Hall measurements at 4.2 K. The 2DEG had a mobility $\sim 5 \times 10^4$ cm^2 V^{-1} s^{-1} and a sheet electron density $\sim 1.2 \times 10^{12}$ cm^{-2}. The electron mean free path of the 2DEG was ~ 1 μm at 4.2 K. The spin coherence length was a few micrometres at this temperature[30]. Side-gated QPC devices were made on the QW structures using high-resolution electron-beam lithography and wet etching on length scale of a few hundred nanometres. The complete device consisted of a Hall bar with the QPC at the centre (see Supplementary Information, A). This allowed a four-probe measurement of the device conductance. A side gate is just a piece of the

2DEG isolated from the conduction channel by deep trenches cut by wet etching. The confining potential of the QPC devices could be made symmetric and asymmetric by applying, respectively, equal ($V_{LG} = V_{RG}$) and unequal ($V_{LG} - V_{RG} \neq 0$) constant bias voltages to the two side gates (Fig. 1a). Side gates were used to create the QPCs because they offer hard-wall confinement that makes it possible to achieve asymmetric confinement of the QPC channel by asymmetric or unequal voltage biasing of the two QPC gates. Asymmetric biasing of top gates, used in the split-gate geometry, mostly shifts the channel laterally. Dry etching was not used because it often introduces defects on the trench walls, which can adversely affect transport. The effective channel width and electron density of a QPC was controlled by appropriately voltage biasing of the side gates. Because it is extremely difficult to control dimensions in wet etching, the widths of the isolation trenches often varied from sample to sample and sometimes for the same sample. For the same reason, the lithographic width of the QPC channel also varied from sample to sample. This was reflected in the varying pinch-off voltage of different devices and gate bias voltages needed for the observation of the conductance plateaus in them. For the same reason, the application of asymmetric bias voltages between the left and right gates of the device did not always produce the corresponding asymmetry in the confining potential. However, the results were reproducible for the same device and variations from device to device were not significant and retained the main features.

Measurements of the four-probe device conductance were carried out on a number of nominally identical QPC devices using a standard lock-in technique with a drain–source bias voltage V_{DS} of between 30 and 100 μV at 17 Hz. Measurements were also made as a function of magnetic field ($\leq$8 T) applied perpendicular to device plane and in-plane parallel to the channel current.

Received 7 May 2009; accepted 24 July 2009; published online 6 September 2009

References

1. Awschalom, D. D. & Flatte, M. E. Challenges for semiconductor spintronics. *Nature Phys.* **3,** 153–159 (2007).
2. Bychkov, Yu. A. & Rashba, E. I. Oscillatory effects and the magnetic susceptibility of carriers in inversion layers. *J. Phys. C* **17,** 6039–6045 (1984).
3. Winkler, R. Spin–orbit coupling effects in two-dimensional electron and hole systems. In *Springer Tracts in Modern Physics* **191** (Springer, 2003).
4. Debald, S. & Emary, C. Spin–orbit driven coherent oscillations in a few-electron quantum dot. *Phys. Rev. Lett.* **94,** 226803 (2005).
5. Flindt, C., Sorensen, A. S. & Flensberg, K. Spin–orbit mediated control of spin qubits. *Phys. Rev. Lett.* **97,** 240501 (2006).
6. Moroz, A. V. & Barnes, C. H. W. Effect of the spin–orbit interaction on the band structure and conductance of quasi-one-dimensional systems. *Phys. Rev. B* **60,** 14272–14285 (1999).
7. Hattori, K. & Okamoto, H. Spin separation and spin Hall effect in quantum wires due to lateral-confinement-induced spin–orbit coupling. *Phys. Rev. B* **74,** 155321 (2006).
8. Xing, Y., Sun, Q.-f., Tang, L. & Hu, J. Accumulation of opposite spins on the transverse edges of a two-dimensional electron gas in a longitudinal electric field. *Phys. Rev. B* **74,** 155313 (2006).
9. Jiang, Y. & Hu, L. Kinetic magnetoelectric effect in a two-dimensional semiconductor strip due to boundary-confinement-induced spin–orbit coupling. *Phys. Rev. B* **74,** 075302 (2006).
10. Dyakonov, M. I. & Khaetskii, A. V. Spin physics in semiconductors. In *Springer Series in Solid-State Sciences* Ch. 8, Vol. 157 (Springer, 2008).
11. Engel, H.-A., Rashba, E. I. & Halperin, B. Theory of spin Hall effects in semiconductors. In *Handbook of Magnetism and Advanced Magnetic Materials* Vol. 5 (John Wiley & Sons, 2007).
12. Kato, Y. K., Myers, Y. C., Gossard, A. C. & Awschalom, D. D. Observation of the spin Hall effect in semiconductors. *Science* **306,** 1910–1913 (2004).
13. Wunderlich, J., Kaestner, B., Sinova, J. & Jungwirth, T. Experimental observation of the spin-Hall effect in a two-dimensional spin–orbit coupled semiconductor system. *Phys. Rev. Lett.* **94,** 047204 (2005).
14. Datta, S. *Electronic Transport in Mesoscopic Systems* (Cambridge Univ. Press, 2005).
15. Van Houten, H., Beenakker, C. W. J. & van Wees, B. J. Nanostructured systems. In *Semiconductors and Semimetals* Ch. 2, Vol. 35 (Academic Press, 1992).
16. Bird, P. J. & Ochiai, Y. Electron spin polarization in nanoscale constrictions. *Science* **303,** 1621–1622 (2004).
17. Büttiker, M. Nanostructured systems. In *Semiconductors and Semimetals* Ch. 4, Vol. 35 (Academic Press, 1992).
18. Beenakker, C. W. J. & van Houten, H. *Solid State Physics: Advances in Research and Applications* Ch. 1, Vol. 44 (Academic Press, 1991).
19. Lassl, A., Schlagheck, P. & Richter, K. Effects of short-range interactions on transport through quantum point contacts: a numerical approach. *Phys. Rev. B* **75,** 045346 (2007).
20. Matveev, K. A. Conductance of a quantum wire at low electron density. *Phys. Rev. B* **70,** 245319 (2004).
21. Fiete, G. A. The spin-incoherent Luttinger liquid. *Rev. Mod. Phys.* **79,** 801–820 (2007).
22. Debray, P., Zverev, V. N., Gurevich, V., Klesse, R. & Newrock, R. S. Coulomb drag between ballistic one-dimensional electron systems. *Semicond. Sci. Technol.* **17,** R21–R34 (2002).
23. Lusakowski, A., Wrobel, J. & Dietl, T. Effect of bulk inversion asymmetry on the Datta-Das transistor. *Phys. Rev. B* **68,** 081201 (2003).
24. Büttiker, M. Four-terminal phase-coherent conductance. *Phys. Rev. Lett.* **57,** 1761–1764 (1986).
25. Wang, C.-K. & Berggren, K.-F. Local spin polarization in ballistic quantum point contacts. *Phys. Rev. B* **57,** 4552–4556 (1997).
26. Hew, W. K. *et al.* Spin-incoherent transport in quantum wires. *Phys. Rev. Lett.* **101,** 036801 (2008).
27. Crook, R. *et al.* Conductance quantization at a half-integer plateau in a symmetric GaAs quantum wire. *Science* **312,** 1359–1362 (2006).
28. Thomas, K. J. *et al.* Interaction effects in a one-dimensional constriction. *Phys. Rev. B* **58,** 4846–4852 (1998).
29. *J. Phys.: Condens. Matter* **20** (2008).
30. Hammer, P. R. & Johnson, M. Detection of spin-polarized electrons into a two-dimensional electron gas. *Phys. Rev. Lett.* **88,** 066806 (2002).

Acknowledgements

P.D. would like to thank J.J. Krich for interesting and useful discussions. The authors are thankful to J. Marcus and R. Schrott for technical help. This work was supported by National Science Foundation (NSF) awards ECCS 0725404 and DMR 0710581.

Author contributions

P.D. conceived and designed the experiments, participated in some measurements, analysed the data and wrote the manuscript. S.M.S.R. made the samples and performed most of the experiments. J.W. and M.C. carried out the NEGF numerical calculations. A.T.N. and S.E.U. conducted theoretical calculations based on free-electron Hamiltonian. S.T.H. and R.S.N. contributed materials, analysis and experimental tools. M. J. contributed materials. M.M. helped with the experiments. All authors discussed the results and commented on the manuscript.

Additional information

Supplementary information accompanies this paper at www.nature.com/naturenanotechnology. Reprints and permission information is available online at http://npg.nature.com/reprintsandpermissions/. Correspondence and requests for materials should be addressed to P.D.